



1 **Isovolumetric replacement and aeolian deposition contributed to Terra calcis**

2 **genesis in Franconia (central Germany)**

3 Bernhard Lucke¹, Helga Kemnitz², Stephan Vitzethum¹

4 ¹Institute of Geography, Friedrich-Alexander University Erlangen-Nürnberg,

5 Wetterkreuz 15, 91058 Erlangen, Germany

6 ² Helga Kemnitz, Katharinenholzstr. 33 B, 14469 Potsdam, Germany

7 Correspondence to: bernhard.lucke@fau.de

8

9 Keywords: Isovolumetric replacement, metasomatism, amorphous clay, illuviation,

10 authigenic clay neoformation, bedrock residue, soils on limestone, Terra calcis,

11 Terra rossa, Terra fusca

12

13

14

15

16

17

18

19



20

21 **Abstract**

22 We investigated Terra calcis on limestone and dolomite in Franconia, as well as the
23 red fill of deep cracks in the rock (*Karstschlotten*). SEM images of the rock-soil
24 transition zones supported by EDS found amorphous clays along fissures that could
25 be products of metasomatic, authigenic clay neoformation within microfossils, calcite,
26 and dolomite grains, or of replacing deposition of amorphous clays inside the calcite,
27 probably due to percolating waters (illuviation). In the SEM-images, the replacement
28 appears as exchange process characterized by substitution of Ca and Mg against Si,
29 Al, and Fe. There is no crystalline clay deposited within rock fissures, and the
30 transition between calcareous minerals and amorphous clay is gradual. This and the
31 presence of Fe let it seem possible that plant roots play a major role for the transport
32 of elements and neoformation of clays, similar to clay pavements along eucalyptus
33 roots in Western Australia. In this context, more or less uniform Fe(d/t) ratios
34 contradicting other weathering indicators could be the result of neoformed
35 phyllosilicates containing Fe³⁺. Bulk soil and bedrock analyses indicate that the solum
36 of the investigated Terra calcis does mainly not represent insoluble bedrock residue.
37 Dust deposition and bioturbation are evident due to sand grains coming from a loess
38 surface cover, which buried pre-existing Terra calcis and contributed to their
39 substrate, apparently supplying quartz and clay-rich pseudosand aggregates.

40

41 **1. Introduction**



42 Until today, there is no general agreement on the genesis of clay-rich red or brown
43 soils on hard limestone in Mediterranean and temperate climates. It has even been
44 suggested that they do not represent true soils but a type of claystone (Merino and
45 Banerjee, 2008). The soil science community largely follows Kubiëna's (1945) model,
46 which proposes that they represent true soils characterized by accumulation of clay.
47 He termed mature profiles 'Terra fusca' (with brown color) and 'Terra rossa' (with red
48 color). Despite the color difference, these soils are characterized by very similar
49 properties. Their close relationship is expressed by the summarizing group name
50 'Terrae calcis' (Kubiëna, 1945), which has been adopted in the German soil
51 classification guidelines (Ad-hoc AG Boden, 2005). Most other soil classification
52 systems do not use such specific terms for clay-rich soils on limestone, but they are
53 applied here as we consider them useful for referring to previous works and
54 discussing the problems connected with the investigation of these soils. For an
55 extensive summary of the literature and a discussion of classification issues, in
56 particular the relation to similar soils in the tropics, see Skowronek (2016). Only a
57 limited part of the literature on the subject can be summarized here; for more
58 comprehensive information see also the reviews in Merino and Banerjee (2008),
59 Trappe (2011), Fedoroff and Courty (2013), and Lucke et al. (2012, 2014).

60

61 **1.1 Parent materials**

62 The debate on the genesis of Terrae calcis starts with the parent material. Leiningen
63 (1930) and Kubiëna (1945) suggested that they resemble mainly the non-soluble
64 residue of calcareous rocks after in-situ dissolution of limestone by meteoric water.
65 However, already these authors contemplated that Terrae calcis may contain a major



66 allochthonous component, possibly mainly from aeolian dust. As outlined by Schmidt
67 et al. (2006), it seems well possible that the contributions of sources vary locally.
68 Studies in Italy (Moresi and Mongelli 1988), China (Shijie et al. 1999; Ji et al. 2004a,
69 2004b), and Turkey (Temur et al. 2009) support the residual theory since the mineral
70 assemblies and geochemistry of these soils are largely similar to the non-calcareous
71 residue of the underlying limestones. However, at other locations substantial
72 differences between soil and rock residue have been found (e.g. Leiningen 1915;
73 Durn et al. 1999). As well, it seems questionable at some locations whether residual
74 formation out of pure limestone could be possible, as this would require the
75 dissolution of huge amounts of rock (Yaalon and Ganor 1973; Merino and Banerjee
76 2008). In this context, long-range transport of Saharan dust was found to play a
77 significant role for soil formation on limestone in a large part of the northern
78 hemisphere (e.g. Muhs, 2001; Muhs et al., 2007; Lucke et al., 2014).

79

80 **1.2 Mechanisms of soil formation: aeolian deposition, bedrock dissolution, and**
81 **illuviation**

82 Closely connected with the question of parent materials is the mechanism of soil
83 formation. Since a steady deposition of Saharan dust takes place in the
84 Mediterranean (Martin et al. 1989), Yaalon and Ganor (1973) suggested that clay-
85 and Fe-rich dust settling with precipitation is the main substrate of most Terra calcis
86 in that area. Saharan dust could even be traced in Terra calcis of the West Indies
87 (Muhs 2001; Muhs et al. 2007; Prognon et al. 2011). Danin et al. (1982) found fossil
88 marks of lichen on limestone under a Terra rossa in Israel, suggesting that the rock
89 had once been exposed to sunlight before being covered by soil. In northern



90 Jordan, Lucke et al. (2014) found a continuous dust signal in soils on different
91 bedrocks and concluded that aeolian deposition must have provided a significant
92 amount of the soil parent material, even though a specific and significant contribution
93 of each different bedrock was clearly indicated as well. Therefore it seems possible
94 that a mixture of aeolian deposition and bedrock weathering can contribute to the
95 genesis of Terra calcis.

96

97 Dissolution of limestone, in particular of clay-rich marls that are often interbedded in
98 calcareous formations, could directly produce a clayey residue (Bronger et al., 1984).
99 During assumed long periods of soil formation, such clay-rich interlayers could have
100 disappeared due to weathering, which is why a divergent composition of the soil and
101 the now underlying limestone does not necessarily prove an allochthonous origin of
102 the solum. In this context, Frolking et al. (1983) and Fedoroff and Courty (2013, and
103 references therein) suggested an illuvial origin of the phyllosilicates. Since smectites
104 may maintain surface acidity even when dispersed in Ca-rich water (Mortland and
105 Raman, 1968), clays might be transported by subsurface waters, trigger limestone
106 dissolution, and accumulate, leading to an effective replacement of limestone by clay.
107 As chert bands in the Galena dolomite in Wisconsin continued through the clays
108 studied by Frolking et al. (1983), this replacement must have taken place
109 isovolumetrically, i.e. not creating larger voids so the chert bands were not disturbed.
110 That the clays had been transported was indicated by oriented coatings on slightly
111 weathered dolomite in greater amounts than could result from in-situ rock dissolution
112 (Frolking et al., 1983).

113

114 **1.3 Metasomatism in *Terrae calcis* genesis**

115 An alternative way of *Terrae calcis* genesis was first suggested by Blanck (1915): the
116 clay-rich substrate could not only be product of bedrock weathering, illuviation, or
117 aeolian deposition, but consist of newly formed (authigenic) clay minerals that
118 replaced the limestone in a pressure-driven metasomatic reaction. In this context,
119 Stephenson (1939) and Ross and Stephenson (1939) discovered fossil mollusks that
120 had apparently been replaced by beidellite and were preserved as clay structures in
121 a limestone bed near Pontotoc, Mississippi. Monroe (1986) reviewed literature
122 regarding the replacement of limestones by clay and conducted a replacement
123 experiment based on circulation of mineralized groundwater through limestone: the
124 experiment failed, but the reported evidence suggested that limestone could indeed
125 be replaced by lime-free clay. These examples, however, do not only refer to the
126 genesis of soils on limestone, but to clay layers within limestone beds and to clay fills
127 of subterranean caves (see also Zippe, 1854; Weyl, 1959; and Fenelon, 1976).

128

129 Maliva and Siever (1988) simulated in the laboratory how chemically completely
130 strange guest minerals can grow in host minerals if a superconcentration of ions
131 precipitating as guest mineral is present: the guest mineral replaces the host mineral
132 in a pressure-driven reaction while maintaining its bedding structures (by 'force of
133 crystallization'). In this context, Zhu and Li (2002) described metasomatic relic
134 bedding structures of the underlying limestone in Terra Rossa in southern China,
135 which could be result of replacement processes as simulated by Maliva and Siever
136 (1988). Merino and Banerjee (2008) investigated thin sections of a 'bleached zone' in
137 the rock-soil transition zone of a Terra rossa in Bloomington, Indiana, and described a



138 'reaction front' that was characterized by partial isovolumetric replacement of
139 limestone by clay, as well as dissolution voids that were associated with the
140 replacement. They calculated a thermodynamic model of the replacement reaction.
141 According to this model, the reaction would on the one hand lead to a pressure-
142 driven isovolumetric replacement of the limestone during authigenic clay
143 neoformation, meaning that the mass balance of soil formation versus bedrock
144 dissolution requires much less limestone for soil formation than the residue model.
145 On the other hand, the reaction would produce acids which could explain the
146 association of Terra rossa with karst, and lead to additional chemical dissolution of
147 limestone with a subsequent mixing of the non-soluble residue with the newly formed
148 clay.

149

150 However, even the comprehensive model presented by Merino and Banerjee (2008)
151 cannot fully explain (authigenic) clay neoformation: one major question is the supply
152 of ions into the rock fissures. Merino and Banerjee (2008) suggested that dissolved
153 aerosols would deliver the necessary elements (mainly Si, Al, and Fe). Banerjee and
154 Merino (2011) further refined the replacement model by accounting for diffusion and
155 infiltration processes. These were based on Amran and Ganor's (2005) dissolution
156 half-lives of smectites in water – for pH 5. However, considering the often neutral to
157 slightly alkaline pH-values as e.g. found by Lucke et al. (2012) for most Terra calcis
158 in northern Jordan, it seems still questionable how ions of Al that are hardly soluble
159 under such conditions could be mobilized from the surface into the rock pores.
160 Metasomatic features could be relic and have formed when soils were completely
161 decalcified, which seems possible since there is evidence that Terra calcis in Jordan



162 were subject to re-calcification in the recent past (Lucke, 2008). However, organic
163 matter might play a role too: Blanck (1915, 1926), Blanck et al. (1928) and Blanck
164 and Oldershausen (1936) proposed that organic acids provide colloids that prevent
165 ions from precipitating even when in contact with calcareous rocks (see also the
166 comprehensive review in Blanck (1930)). This idea could explain why red soils are
167 largely absent on calcareous rocks of temperate zones: due to the much lower
168 humus contents of soils in Mediterranean climates, ions must precipitate when
169 reaching the calcareous rocks, but not if larger humus concentrations are present
170 (Blanck, 1915). It could mean that Terra fusca might be less a product of replacement
171 processes than Terra rossa due to the usually significantly higher contents of organic
172 matter in Terra fusca.

173

174 However, other ion transport mechanisms seem possible too: Reifenberg (1927,
175 1947) argued that silicic acids, and not humus, provided the colloid that prevented
176 flocculation of sesquioxides and growth of minerals before ions entered the rock
177 pores. Reifenberg (1947) suggested further that the source of the ions in semi-arid
178 areas might not be the soil surface, but ascending waters from the rocks. Lucke et al.
179 (2012) suggested that plant roots might supply the necessary ions to the rock pores,
180 based on the observation that plant roots can often be found in rock fissures, and on
181 the reported neoformation of clays associated with root exudates of mallee eucalypts
182 in geochemically completely different sand dunes that was observed by Verboom et
183 al. (2009). This casts some doubts on a possible connection of organic matter and
184 colors of *Terrae calcis*, although Terefe et al. (2008) suggested that repeated
185 vegetation fires and thus organic matter could cause long-term red coloration.



186

187 **1.4 Colors of Terra calcis**

188 Various ideas have been brought forward to explain the prevalence of brown and red
189 colors of Terra calcis. The red color of Terra rossae could be inherited from the
190 insoluble limestone residue (Bronger et al., 1984), could have formed during
191 pedogenensis under warmer and more humid climates of the past (Klinge, 1958), or
192 simply result from oxidized Fe^{2+} that was released during the weathering of
193 carbonate rocks (Meyer, 1979). Schwertmann et al. (1982) suggested that rapid
194 wetting-drying cycles as often prevailing in Mediterranean climates and on well-
195 drained karst areas can lead to recrystallization of ferrihydrite as hematite, which
196 gives red color even when present in only small concentrations. Although this
197 process could not yet be modeled in the laboratory, Barrón and Torrent (2002)
198 showed that ferrihydrite can transform into maghemite under presence of phosphate
199 or other ligands capable of exchange of Fe-OH surface groups. Based on this,
200 Torrent et al. (2006) suggested that maghemite formation is a precursor of hematite
201 during ferrihydrite transformation in aerobic soils poor in organic matter, which
202 matches evidence collected by Lucke and Sprafke (2015) along a climatic transect in
203 northern Jordan. In contrast, the prevailing brown colors of temperate areas seem
204 connected to less pronounced moisture differences, and it has been suggested that a
205 change to moister and cooler conditions could have caused xanthization of formerly
206 red soils, meaning that red-colored hematite would change to goethite (Boero and
207 Schwertmann, 1987).

208



209 **2. Genesis of Terra calcis in Franconia (central Germany)**

210 Franconia hosts widespread limestone plateaus which are partially covered by
211 brownish and reddish Terra calcis (locally called *Alblehm*). These plateaus were
212 mostly not glaciated, but situated in a periglacial environment during the Pleistocene.
213 Terraes calcis are partly present at the surface, and partly buried by loess and sands,
214 and can be found as fills of deep cracks and dolines in the limestones. While the
215 plateau soils are mostly brown, the crack fills are often characterized by intense red
216 colors. Their environmental significance is debated. According to Mückenhausen et
217 al. (1975), red infillings in limestone cracks could be relics of a former soil cover,
218 possibly of *Terrae rossae* or *Ferralsols* from the Cretaceous or Tertiary, which was
219 eroded on the surface but preserved in the cracks. Zech et al. (1979) investigated red
220 clayey fills in karst cracks of Franconia and concluded that their color testifies to
221 formation during warmer and moister tropical climates of the past. This is supported
222 by higher amounts of kaolinite in the clay infillings compared to the residue of the
223 surrounding bedrock. However, in the light of theories of *Terrae calcis* formation
224 discussed above, it seems also possible that the crack fills are products of illuviation,
225 or clay neoformation – and the different color might be explained by divergent organic
226 matter contents, since the cracks are not connected to the actual surface.

227

228 In this context, “powdery” layers of CaCO_3 of approximately 1 mm thickness have
229 been described by Trappe (2011: 96) for the rock-soil transition zones of *Terrae calcis*
230 in our studied area in Franconia, who interpreted them as potential evidence of
231 insoluble limestone residue contributing to solum formation. However, the limestones
232 are very pure: Häusler and Niederbudde (1992) estimated that about 3 mm of soil



233 cover could have formed out of the respective limestone residue during the
234 Holocene, meaning that Terra calcis such as the ones investigated in this study
235 would have experienced about 2.7 Ma of soil development under the current climate
236 without erosion in order to reach the present depth. Trappe (2011) argued in this
237 context that the Terra calcis and crack fillings in Franconia represent mixed
238 sediments, largely stemming from weathered chalk layers, since the limestones
239 produce too little residue. However, no high-resolution study of the micromorphology
240 of these soils and their transition zones to bedrock was yet accomplished.

241
242 Although a final explanation of the mechanisms of the metasomatic replacement
243 process cannot yet be offered, there is growing evidence that in-situ neoformation of
244 clay can contribute to the formation of clay-rich soils on limestone (see e.g. Feng et
245 al. (2009) and the review by Laverty (2012). Key evidence for isovolumetric
246 replacement are 'shadows' of the original rock structures that are preserved in the
247 soil-rock transition zone, in particular microfossils partially consisting of clay. If
248 neoformation of clay minerals in limestone took or takes place, a spatially precise
249 approach focusing on partially replaced microfossils can track it. And if partially
250 replaced microfossils can be confirmed for Terra fuscae, it would suggest that
251 metasomatic processes are less dependent on organic matter than suggested by
252 Blanck (1915). Therefore we studied the micromorphology of the rock-soil transition
253 zones of two Terra fuscae and a limestone crack filled with Terra rossa in Franconia
254 with regard to the presence of partially replaced microfossils and minerals. In
255 addition, bulk samples of the substrate and the microsurfaces of sand grains were
256 investigated. These areas had been studied before by Blanck and Oldershausen



257 (1936), and we attempted to re-visit some of their investigation sites in order to honor
258 their prior efforts, applying now available more advanced methods of analysis.

259

260 **3. The sampled profiles**

261 From a total of five studied sites, two are presented here. The first profile 'Fricke' is
262 located in a quarry approximately 4 km southeast of the town Weißenburg i. Bayern
263 on top of a limestone plateau (N 49° 00' 36.6“, E 11° 01' 35.7“, see figs. 1, 2a and b).
264 Here a thick hard limestone from the upper Jurassic/Malm δ containing *Ammonites*
265 *pseudomutabilis* (locally called *Weißenburger Marmor*) is exposed, which is well-
266 suited for construction and exported worldwide. The rock has vertical cracks that are
267 filled with uniform red clay which was already observed and studied by Blanck and
268 Oldershausen (1936). We named our profile according to the designation given by
269 these authors, although the exact part of the limestone quarry which they studied has
270 been removed by constant quarrying during the past 80 years. In the studied profile,
271 the clay-filled cracks are not connected to the present surface, but interrupted by
272 another layer of hard limestone. On this layer a zone of intense rock weathering (see
273 fig. 2b) resembles the bedrock of soil formation on the current surface. It can
274 however not be excluded that there was a connection of the crack to the surface in
275 the front of the profile that was removed by quarrying.

276

277 The soil developed at the surface can be classified as Cambisol (Siltic) according to
278 the World Reference Base of Soil Resources (WRB 2014). According to the German
279 soil classification system (Ad-hoc AG Boden 2005), a Braunerde-Terra fusca is
280 present: the lower part of the profile could be described as Terra fusca, which



281 gradually changes into a Braunerde formed out of loess in the upper part. Soil
282 horizons were classified according to the German system (Ad-hoc AG Boden 2005,
283 see figs. 2a and b). There is a gradual transition from a dark-brown, clay-rich Terra
284 fusca horizon (II TBv) to a bright yellowish, silty Bv horizon that apparently resembles
285 loess which at some time buried a prior developed Terra fusca. Roots were present
286 throughout the whole profile and even in the deepest crack fillings. Although we
287 sampled the whole profile for bulk soil analysis, only the soil-rock transition zone of
288 the red clay in the cracks was studied by micromorphology. Bulk samples of the crack
289 infillings were taken in the upper and lower part of the crack (samples III Tu (1) and
290 (2). The crack fillings are homogeneous and no horizons or indicators of fluvial
291 deposition could be observed (fig. 2c). As well, the bedrock was sampled and
292 analyzed for calcium carbonate, total element contents, residue particle sizes, and
293 residue color.

294

295

296 Figure 1

297 Figure 2a

298 Figure 2b

299 Figure 2c

300

301 The second profile 'Schwaighauser Forst' is located at the eastern border of
302 Franconia, locally called *Bruchschollenland*, an area characterised by strong faulting
303 and dislocation of geological units. Therefore very different lithologies are exposed at
304 the surface in small areas, and some volcanic activity about 50 km to the east was
305 associated with the faulting. The studied soil represents an Epileptic Cambisol



306 (clayic) according to the WRB (WRB 2014). According to the German soil
307 classification system (Ad-hoc AG Boden, 2005) it can be classified as Terra fusca. It
308 is located in an educational soil trail (N 49° 05' 10.7", E12° 00' 12.7") north-west of
309 the city of Regensburg (TUM 2014), formed on dolomitic limestone from the Upper
310 Jurassic/Malm ϵ - ζ . At this profile, a loess cover is not discernible, but may have
311 eroded since the solum is much shallower than at the first profile (figs. 3a and 3b).
312 Roots were present throughout the whole profile. Apart from each horizon, the
313 bedrock was analyzed for calcium carbonate, total element contents, residue particle
314 sizes, and residue color.

315

316

317 Figure 3a

318 Figure 3b

319

320 **4. Methods**

321 Our main aim was to check whether partially replaced microfossils can be found in
322 the rock-soil transition zones of the sampled profiles, supported by some analyses of
323 bulk soil and bedrock residue in order to describe soil development intensity.
324 Micromorphological samples were taken from the transition of the unweathered
325 bedrock to the clay of *Terrae calcis*, including several samples covering the whole
326 distance from the apparently unweathered rock till clay aggregates of the solum. Thin
327 but stable metal containers were placed on the transition of soil and rock and the
328 samples slowly cut out with a knife. After freeze drying, samples were stabilized using
329 Araldite A2020 epoxy resin. The thin sections received a diamond-polishing and were



330 carbon coated. After optical analysis, microanalysis was done with a high resolution
331 field-emission scanning electron microscope (FESEM; Carl Zeiss Ultra 55 Plus),
332 equipped with an energy-dispersive system (EDS) by Thermo Fisher Scientific. In
333 contrast to only optical analysis, scanning electron microscope analysis with EDS
334 permits determining the geochemistry of the studied areas. This can allow detecting
335 minerals that appear amorphous to X-ray diffraction and optical studies. In addition,
336 large allochthonous clays such as biotite grains can be misinterpreted as in-situ
337 formed minerals as shown by Lucke et al. (2012) if only optical analysis is applied,
338 and the scanning electron microscope (SEM) allows investigating smaller features at
339 scales of nanometers.

340

341 General soil analyses determined calcium carbonate and organic carbon contents
342 with a Leco TrueSpec C-N analyser measuring samples before and after ignition of
343 organic matter at 430 °C for two hours (Schlichting et al., 1995), based on the
344 assumption that the remaining content of C represents carbon bound in calcium
345 carbonate. The dolomite content of the dolomitic limestone was estimated from the
346 residue mass after dissolution of the calcareous part of the rock with 10% HCl. Soil
347 color of dry soil samples and the color of dried bedrock residue after dissolution with
348 10% HCl were determined using the Munsell color chart, and redness ratings
349 calculated according to Hurst (1977). In order to control whether the treatment of the
350 rock with 10% hydrochloric acid could lead to a loss of red color of the residue,
351 samples of the Terra rossa limestone crack infillings were simultaneously treated with
352 the same amount of acid during the same time of bedrock dissolution, but no color
353 change could be observed. Analysis of clay minerals would require rock dissolution



354 with weaker acids in order to exclude alteration of the minerals due to acid treatment
355 (Ostrom, 1961; Rabenhorst and Wilding, 1984), but since only the texture and color
356 of the residue were studied, faster treatment with stronger acid was chosen.

357

358 Pedogenic iron oxides were extracted with sodium dithionite at room temperature
359 according to Holmgren (Schlichting et al. 1995), and the iron contents measured with
360 an ICP Spectrometer (Thermo Scientific iCAP 6200 Duo). In case samples contained
361 more than 4% CaCO_3 , particle sizes were analyzed after removing CaCO_3 with 10%
362 hydrochloric acid and washing the samples until conductivity dropped below 200 μS .
363 These and the other samples containing less than 4% CaCO_3 were then dispersed
364 with sodium hexametaphosphate ($\text{Na}_4\text{P}_2\text{O}_7$) and shaken overnight (Schlichting et al.,
365 1995). Wet sieving determined the sand fraction according to DIN 19683 (1973),
366 while the smaller particles were analysed with a Sedigraph (Micromeritics). For total
367 element analysis by X-ray fluorescence, we determined the loss on ignition (LOI) by
368 weighing the powdered samples before and after drying: 1) 12 hours at 105 °C in a
369 cabinet dryer and 2) 12 hours at 1030°C in a muffle furnace. Major element oxides
370 (SiO_2 , TiO_2 , Al_2O_3 , FeO , MnO , MgO , CaO , Na_2O , K_2O , P_2O_5) and selected trace
371 elements (Ba, Cr, Ga, Nb, Ni, Pb, Rb, Sr, Th, V, Y, Zn, Zr) were measured with a
372 Spectro XEPOS at the GeoZentrum Nordbayern. Precision and accuracy are
373 generally better than 0.9% and 5%, respectively.

374

375 **5. Results**

376 **5.1 Micromorphology of the rock-soil transition zones**



377 Limestone beddings partially consisting of clay could be found in the rock-soil
378 transition zones of both studied profiles. Figure 4 shows a calcite grain partially
379 consisting of clay in the 'powdery' (see Trappe, 2011) transition zone of about 1 mm
380 thickness, directly between the red clay and the limestone in the profile 'Fricke'. It
381 appears that a prograding solution is encompassed simultaneously by the formation
382 of clay. As shown by the serrated grain rim in fig. 4 (upper part), exchange seems to
383 occur along zones of potential permeability such as fine fissures, at grain contacts, or
384 through pores. That part of the calcite already consists of clay is shown by the
385 spectral image in fig. 4 (lower part). Although secondary calcite needles were noted
386 in some fissures, no clay could be observed in the pores: there are no clay films
387 suggesting that allochthonous clay has been transported into the rock. As well, the
388 original form of the calcite grain is so well preserved that the clay cannot be of
389 allochthonous origin, but must represent the in-situ limestone, and there is no
390 structure discernible that could be attributed to micro-clay beddings deposited during
391 limestone formation. Conclusively, bedrock weathering may not simply proceed by
392 chemical reaction processes which create voids in the rock due to chemical
393 dissolution, but clay neoformation and rock dissolution could be part of the same
394 process as suggested by Merino and Banerjee (2008).

395

396 Figure 4

397

398 About 1 cm deeper into the limestone, it appears rather unaltered to the naked eye
399 and remains of biogenic shells can be observed macroscopically. But there are also



400 some small reddish lines. Analysis with the SEM confirmed that some of these lines
401 represent clay, which is partly present inside microfossils. Figure 5 shows a biogenic
402 relict (probably alga or foram) partially consisting of clay which is surrounded by still
403 largely unweathered limestone. Again, there is no evidence that the clay was
404 transported into the microfossil, since the outer shell is still closed and consists of
405 calcium carbonate. Though the outer shell seems preserved and closed, consisting of
406 calcium carbonate, one has to account for the three-dimensionality of the organism
407 and a high likelihood of pores. But the apparently amorphous structure of the clay
408 inside the microfossil argues against allochthonous clay minerals. Furthermore, it still
409 contains significant amounts of the former calcium carbonate filling (see spectral
410 images in fig. 5).

411

412 Figure 5

413

414 The Terra fusca of the Schwaighauser Forst profile formed on a dolomitic limestone
415 that is characterized by low density of microfossil remains in the rock. Yet, some
416 microfossils partially consisting of clay could be observed in the direct soil-rock
417 transition zone, inside the rock in about 10 µm distance to the border of the limestone
418 as shown in figure 6. This microfossil is characterized by high contents of magnesium
419 corresponding to bedrock chemistry. The minor Si peak that is detected in the inner
420 section might either derive from naturally implemented traces of silica or indicates
421 authigenic neoformation of clay, too.

422



423 Figure 6

424

425 In a clay-filled fissure of the dolomite rock beneath the Terra fusca, we investigated
426 serrated structures partly showing areas that appear darker in the SEM. Figure 7
427 shows a calcite grain directly bordering the clay-filled fissure. The EDS-analyses
428 show how the calcite at the edge starting to disintegrate contains already some silica
429 and magnesium (point 1). Since magnesium might also be a component of the
430 carbonate, one might argue for an analytical effect because of the beam size. This,
431 however, does not fall below under 1.5 μm in diametre in this case, such that the
432 analyzed microvolume is restricted to the calcitic part of the grain. Comparison with
433 the elemental composition of the clayey crack fill with the clay in the fissure (point 2),
434 in particular regarding the Al:Si ratios, shows a clear clay mineral signal with a
435 strongly reduced calcium content.

436

437 Figure 7

438

439 The replacement of calcium and magnesium by clay seems further indicated by an
440 EDS cross-section (line scan) through a dolomite grain about 50 μm deeper into the
441 bedrock (fig. 8). A darker domain of the dolomite proves as clay, characterized by a
442 significant decline of Ca and Mg, while Si, Al, and Fe increase. However, this clay
443 seems not yet fully de-calcified, and appears merely like an amorphous gel. We have
444 not been able to identify crystallinity, and the area is too small to be determined by
445 optical analysis, which would misinterpret it as calcite.



446

447 Figure 8

448

449 **5.2 Bulk soil analysis**

450 Results of both profiles are summarized in table 1. It can be observed that the Terra
451 rossa red crack filling samples of the Fricke profile [samples Tu(1) and Tu(2)] are
452 more or less identical, confirming the field impression that no horizons or deposition
453 patterns are present in the cracks. However, the fills are distinct from the Terrae
454 fuscae: apart from the red color, values of dithionite soluble iron are elevated. As well,
455 values of oxalate-soluble silicium are elevated, pointing to a higher content of
456 amorphous silica than in the Terrae fuscae.

457

458 The Terra rossa crack fillings are characterized by higher clay contents than the
459 Terrae fuscae, but also by a higher sand content than the bedrock residue. The latter
460 could to some degree be connected with the acid treatment to dissolve the rock. The
461 crack infillings received no acid pre-treatment before grain size analysis due to low
462 CaCO_3 -contents, and since acid-pretreatment also removes calcite sand grains
463 (Lucke and Schmidt, 2015), sand contents of crack infillings and bedrock residue are
464 not directly comparable. Calcite sand grains in the Terra rossa-filled cracks might
465 represent micro-“floaters” as suggested by Meert et al. (2009) regarding limestone
466 blocks of larger scale “floating” in the Bloomington Terra Rossa in Indiana. However,
467 the majority of sand grains in the crack fillings consist largely of rounded quartz
468 grains of the finer sand fractions (6% coarse sand, 47% middle sand, 47% fine sand),



469 with some equally rounded black grains that might reflect a primary detrital input.
470 While some quartz grains of the coarse-sand fraction show densely set small V-
471 shaped marks typical for aeolian transport during loess deposition (fig. 9), there are
472 also grains being completely covered by clay minerals that are unsuitable for a grain
473 surface characterization (fig. 10).

474

475 Figure 9

476 Figure 10

477

478 This suggests that allochthonous material, including grains transported with the
479 overlying loess, was involved in the formation of the crack fills. The very similar sand
480 contents in the two samples of crack fillings point to a very homogeneous distribution
481 of sand within the cracks, which is in agreement with the field impression and other
482 results of bulk soil analysis. The strongly elevated sand contents compared to the
483 bedrock residue argue against inheritance from rock dissolution, and the absence of
484 fluvial sorting and very homogeneous distribution of sand grains in the clay argue
485 against fluvial deposition of the crack fills.

486

487 Although the crack fillings were affected by loess deposition on the surface, lab
488 results support the field impression that two different soil formation processes took
489 place. Very similar Ti/Zr values of the lower Terra fusca at the profile Fricke [sample II
490 TCv] and the Terra rossa red clay crack fillings let a common parent material seem



491 possible, which is different from the limestone residue. Although it cannot be ruled out
492 that clay-rich beds - now removed due to weathering - provided residue contributing
493 to soil formation, the analyzed rock sample suggests that neither the buried Terra
494 fusca nor the Terra rossa crack fillings originated from the residue of the now
495 adjacent limestone.

496

497 Table 1

498

499 The limestone and dolomitic limestone proved to be very pure with acid-soluble
500 fractions of 98.1% and 99.99%. Their residue is extremely clay-rich compared to the
501 crack fillings and the II TCv sample of the Terra fusca of the Schwaighauser Forst
502 profile. As well, Ti/Zr ratios are different between rocks and soils, although there are
503 gradients visible in the profiles. These supports the field impression that loess was
504 deposited on the surface and mixed with pre-existing Terra calcis, leading to a
505 gradual lowering of the Ti/Zr ratio towards the tops of the profiles. Even though there
506 was no loess addition apparent in the Schwaighauser Forst profile, particle sizes
507 clearly support that silty material was mixed into the soil. This is further stressed by
508 the absolute content of dithionite-soluble iron, indicating that less weathered material
509 was deposited on top of the profiles. However, in contrast to the other parameters,
510 Fe(d/t) ratios suggest that weathering intensity remained nearly constant through the
511 profiles. This is not an uncommon phenomenon: Günster (1999) and Lucke (2008)
512 encountered similar Fe(d/t) values in Terra calcis of southern Spain and northern
513 Jordan, which did not match other indicators of pedogenesis intensity. It could be



514 explained assuming that some of the dithionite-extractable iron in well-developed
515 Terra calcis might not result from oxidation of Fe^{2+} during weathering, but represents
516 pre-weathered Fe^{3+} -rich phyllosilicates released from the rock residue – or enters the
517 system from outside as Fe^{3+} . The latter might be happening when mineral
518 neoformation due to isovolumetric replacement, illuviation of amorphous clay, or dust
519 deposition contribute to soil formation.

520

521 The contents of organic matter and calcium carbonate are mostly low throughout the
522 profiles. The Terra fuscae seem to contain more organic material than the Terra
523 rossa of the crack fillings, which matches expectations. However, in the profile Fricke
524 only the Ah-horizon contains a relatively high amount of organic matter, while the
525 lower horizons have only little more than the crack fillings. On the one hand, it is
526 surprising that the crack fillings do contain organic matter at all, since they seemed
527 disconnected from the present surface. On the other hand, roots occur in limestone
528 fissures even in great depth, so that the organic matter present in the limestone
529 cracks most likely represents roots.

530

531 pH values are mostly neutral – only in the upper part of the Fricke profile values
532 between 4.5 – 5.5 can be observed, but this matches the high amount of organic
533 matter and the field impression that the parent material of this part of the profile is
534 mainly decalcified loess. There is no difference of the pH values of the red clay
535 infillings of the limestone cracks and the Terra fusca of Schwaighauser Forst. In this



536 context, the bedrock residue of both profiles is not red, but brown and greyish brown.

537 Therefore it seems unlikely that the color was inherited from the bedrock residue.

538

539 Last but not least, calcium carbonate values are low throughout all profiles, except in
540 the TCv horizon of the Terra fusca developed on dolomitic limestone in the
541 Schwaighauser Forst profile. Apparently the dolomite has not completely been
542 weathered, and thin sections showed that calcium carbonate re-precipitated in the
543 soil matrix.

544

545 **6. Discussion**

546 **6.1 Parent materials**

547 It is evident that the investigated Terra fuscae and Terra rossa crack fillings cannot
548 represent only bedrock residue. This is indicated by the differences of color and
549 particle size between the soils and bedrock residues. In addition, grains of the sand
550 fraction of the crack fills confirm that there has been a deposition of material from the
551 covering loess into the fills. Moreover, at the microscale it seems possible that
552 metasomatic processes took or take place in the direct rock-soil transition zones of all
553 investigated profiles, leading to replacement of bedrock with clay in the
554 approximately outer 50 µm of the bedrock. In this context, clay neoformation seems a
555 gradual replacement process: the SEM observations point to a gradual exchange of
556 Ca and Mg against Si, Al, and Fe. Newly formed (authigenic) clay appears as gel-like
557 material, distributed along calcite as well as dolomite grain boundaries, or in patches
558 and small domains within and around decaying carbonate rock and its incorporated



559 microfossils. No crystallinity can be identified. Often, the contact between
560 calcite/dolomite and clay is present as an irregularly prograding, indenting front,
561 which is important to note as it constrains a simultaneous transformation from one
562 mineral to the other.

563

564 **6.2 Amorphous (metasomatic?) clays**

565 All clays occurring in microfossils and minerals are connected to grain boundaries,
566 fissures, and pores occurring within the soil-rock transition zone, while the unaltered
567 rock in areas remote from fissures lacks those observations. Thus underlines a
568 correlation between the replacement process and the movement of solutions in the
569 rock. There are no deposition structures such as oriented crystalline clay layers that
570 could be connected with illuviation. However, it cannot be ruled out that amorphous
571 clay is transported into the transition zones. If amorphous phyllosilicates are
572 transported by percolating waters as proposed by Frolking et al. (1983), they are
573 apparently not accumulating in voids, but adhere to calcite and dolomite grain
574 surfaces. Most of the observed phyllosilicates contain iron, implying that it has either
575 been transported as coating of amorphous clay minerals, or as ions. At few locations
576 secondary CaCO_3 needles precipitated near fissures, suggesting at least temporary
577 presence of solutes in the pore water. There is no discernible microstructural
578 difference between Terra fusca and Terra rossa in the scanning electron microscope
579 images.

580

581 **6.3 Bulk soil analysis**



582 Bulk soil analyses let it seem possible that replacement and/or transport of
583 amorphous clays contributed more to the genesis of Terra rossa in the crack fillings
584 since the contents of oxalate-soluble silica are higher in the Terra rossa. However,
585 there is no reason to assume that higher contents of organic matter in Terra fuscae
586 prevent or strongly limit processes of metasomatism and/or transport of amorphous
587 clays. This argues against Blanck's (1915) suggestion that topsoil organic matter
588 contents play a role in Terra calcis genesis. In this context, the very similar pH
589 values of the Terra rossa crack infillings and the Terra fuscae suggests that the pH
590 value does not play a major role for the development of red or brown color – at least
591 if assuming that the actual pH is relevant for amorphous clays and the formation of
592 replacement features. Similarly, it does not seem probable that organic matter
593 contents affect the color of Terra calcis since the differences between Terra rossa
594 and Terra fusca are not very pronounced, at least in the Fricke profile.

595

596 The Terra rossa and Terra fuscae are characterized by similar particle sizes. At both
597 sites the particle sizes indicate deposition of loess in the upper part of the profiles.
598 Since the bedrock residue is at both profiles characterized by much finer particle
599 sizes, it seems unlikely that the residue of bedrock dissolution contributed a major
600 part of the solum. This is further supported by the Ti/Zr ratios, which are different
601 between the rock and overlying soil. They indicate that loess did not provide the main
602 parent material of Terra calcis genesis, but altered soil properties during deposition
603 on pre-existing soils. There is a strong similarity between the Terra rossa crack fillings
604 and lower part of the Terra fusca in the Fricke profile, which lets it seem possible that
605 similar parent material was involved in formation of these soils. Whether this was



606 aeolian dust cannot be deducted from the available data: the Ti/Zr ratios support the
607 impression of loess deposition and mixing only into the upper part of the profiles, but
608 do not deliver insights into possible aeolian parent materials of earlier pedogenesis.
609 Here the dominant finer sand fractions in the Terra rossa crack fillings, as well as the
610 absence of horizons or depositional structures connected with fluvial sediments,
611 support that an early phase of aeolian sedimentation might have been connected
612 with formation of the red fills. These aerosols could have delivered elements driving
613 replacement reactions as well. The very homogeneous distribution of sand grains in
614 the clay of the crack fill speaks against fluvial sorting patterns. The most likely
615 explanation how sand grains entered the cracks seem root channels and shrink-swell
616 cracks in the clay, while the dominance of the finer sand fractions indicates an
617 aeolian source of the grains – possibly largely from loess deposition.

618

619 Similar to the sand, small aggregates consisting of silt and clay could have been
620 transported into the limestone cracks by wind and bioturbation. Fedoroff and Courty
621 (2013) suggested that wind-blown transport of clayey pseudosands from pre-existing
622 red soils contributed to the genesis of many Terra calcis, possibly following events
623 of sudden and considerable pressure such as airbursts during cosmic impacts. Apart
624 from the presented sand grains, we could not observe pseudosand structures in the
625 clay matrix of the studied profile, but they could have been lost during shrink-swell
626 processes. Such processes could also have blurred clay illuviation cutans in the
627 solum (Fedoroff and Courty, 2013).

628



629 One major question is the iron dynamics of the studied soils. The absolute amounts
630 of dithionite-soluble iron suggest that the Terra rossa crack infillings contain more
631 pedogenic iron than the Terrae fuscae. This could indicate that iron dynamics are
632 connected with organic matter contents as suggested by Blanck (1915), since higher
633 contents of dithionite-soluble iron seem to correspond to lower values of organic
634 matter. However, there is no correlation to the pH-value, and more important, no
635 correspondence to the Fe(d/t) ratio. According to Cornell and Schwertmann (2003),
636 this ratio can be interpreted as indicator of Fe^{2+} oxidation to Fe^{3+} , which is usually a
637 marker of mineral weathering and pedogenesis. Since it remains more or less
638 constant in nearly all investigated samples, this essentially contradicts the impression
639 of stronger weathering given by the particle sizes in the lower part of the profiles. The
640 Fe(d/t) ratio has been problematic in other studies of Terra calcis soil development.
641 For example, Günster (1999) suggested that it should be modified by the clay content
642 in order to achieve reasonable results not contradicting other indicators of soil
643 development intensity, since he observed a strong correlation of Fe_d -contents with
644 clay in southern Spain. In contrast, Lucke (2008) found that the contents of Fe_d in
645 Terra rossae of northern Jordan showed some correlation to contents of calcium
646 carbonate, and suggested modifying the index with the calcium carbonate content.

647

648 At the studied profiles in Franconia, however, those two modifications are
649 inapplicable since there is no apparent connection between the contents of iron,
650 calcium carbonate, and particle sizes. Since limestone might contain threevalent iron
651 from sediments, the problematic Fe(d/t) values could be explained by pre-weathered
652 bedrock residue. However, in light of our microstructural and analytical results



653 regarding clay neoformation, a different hypothesis is formulated here: that not only
654 'classical' pedogenesis is connected with the Fe(d/t) ratios in Terra calcis. Instead,
655 we regard it possible that the iron content is affected by neoformation of
656 phyllosilicates involving the transport of external Fe^{3+} ions. If we assume that
657 aluminium, which is hardly soluble at neutral pH values, can be transported into the
658 rock-soil transition zone, it seems possible that iron can be transported too, possibly
659 involving the same transport mechanism. In this context, iron transport by thermal
660 waters due to volcanism seems possible in the geological context of the
661 Schwaighauser Forst profile, although there is no direct evidence for that. However,
662 the Fricke profile seems located rather far from zones of volcanic activity, and there
663 are so far no clear indications of volcanic ash deposition.

664

665 It seems certain that metasomatism and/or illuviation of amorphous clays can
666 contribute to Terra calcis genesis regardless of the climate or temperature. Further, it
667 seems likely that the development of red color is connected with strong wetting and
668 drying cycles as suggested by Cornell and Schwertmann (2003). Related to this, we
669 think it possible that the Terra rossa of the limestone crack infillings of the Fricke
670 profile was subject to stronger climatic switches than the upper part of the profile - or
671 only the upper part was subject to xanthization.

672

673 **6.4 Evidence from related studies**

674 Küfmann (2008) observed that the thickness of Terra calcis in the northern
675 calcareous Alps was linearly correlated to the proportion of insoluble residue of



676 limestone bedrock. However, her calculation of the possible contribution of bedrock
677 residue (about 20%) and aeolian deposits (about 50%) during the Holocene could
678 explain only about 70% of the present soil thickness. Longer time periods of soil
679 formation do not seem probable since the Alps were glaciated during the Pleistocene.
680 The missing part might be the contribution by isovolumetric replacement and/or
681 illuviation of amorphous clays, which could also explain the positive correlation of soil
682 depth with bedrock residue. Since the metasomatic model of Merino and Banerjee
683 (2008) predicts that acids are produced during the replacement process, the non-
684 soluble residue of the limestone rocks also contributes to soil development: more
685 residue will be released in less pure limestones, leading to quicker build-up of the
686 profile.

687

688 For now it has to be left open how the transport mechanism leading to
689 superconcentration of ions in the rock pores can be explained, but we think that roots
690 which are present in larger rock fissures and even in the deepest part of the studied
691 clay-filled cracks seem the most probable transport agents. Verboom et al. (2009)
692 found that roots of eucalypts colonizing sand dunes in Western Australia were
693 capable of transporting Al, Fe, and Si, leading to the construction of clay pavements
694 along the roots in a geochemically alien surrounding. The same elements were found
695 in the amorphous clays of our studies, which indicates that these probably represent
696 largely authigenic, newly formed clay minerals that stem from reactions triggered by
697 plant roots.

698



699 Our study suggests that bulk soil and rock analyses alone can deliver only limited
700 insight into Terra calcis development, at least at sites where clay neoformation
701 contributes significantly to the genesis of these soils. It appears that bedrock
702 weathering does not only proceed by chemical reaction processes which create voids
703 in the rock due to dissolution, but that neoformation of new minerals and rock
704 dissolution can be part of the same process. Unfortunately it was not yet possible to
705 study the mineralogy of the crystalline clays. In the future, a better understanding of
706 mineral crystallization out of the observed apparently amorphous clays could help to
707 better explain the factors controlling Terra calcis formation.

708

709 **7. Conclusions**

710 Our study found amorphous clays in the direct rock-soil transition zones of all studied
711 profiles. Although it cannot be stated whether these are ongoing or relic features, it
712 can be concluded that:

713 - Isovolumetric replacement of limestone due to metasomatism and/or illuviation of
714 amorphous clays took place in Terra fuscae as well as Terra rossae in
715 Franconia.

716 - Current topsoil organic matter contents and soil color apparently do not matter for
717 the occurrence of these features.

718 - Amorphous clays are observed only close to micropassages in the rock-soil
719 transition zone, suggesting that rock pore solutions play a role for their occurrence.
720 These clays do not fill voids, but are present only in contact with calcite structures.



721 - There is a gradual transition between calcareous minerals and amorphous clay, and
722 no sharp boundary as would be expected from dissolution and deposition processes.

723 - The presence of Fe suggests that replacing amorphous clays are either iron-coated
724 during illuviation, or Fe-ions are transported in a similar way as Al and Si. Since the
725 same elements can be found in clay pavements around Eucalyptus roots in Western
726 Australia, this suggests that root activity might play a major role for the formation of
727 amorphous clays.

728 - No crystalline illuvial clay could be observed in pores, but allochthonous sand was
729 deposited into the limestone cracks during loess deposition by wind and bioturbation.
730 It seems well possible that pseudosand clay aggregates contributed to the solum.
731 These might explain a part of the substrate, but not the amorphous clays observed in
732 the rock-soil transition zones.

733 - The investigated Terra calcis represent true soils and not claystones, since they
734 contain a significant share of allochthonous material and are subject to processes
735 induced by plants – which, by definition, means that pedogenesis takes place.

736

737 We conclude that replacement processes can contribute to the genesis of Terra calcis in Franconia. It is not yet possible to quantify their contribution, and the
738 mechanisms of the process cannot yet fully be explained. However, further studies
739 should consider the possible role of plants for authigenic clay neoformation in Terra calcis
740 genesis.

742

743 **References**

744 Ad-hoc AG Boden, 2005. Bodenkundliche Kartieranleitung. 5th edn. Stuttgart,
745 Schweizerbart.

746 Amram, K., and Ganor, J., 2005. The combined effect of pH and temperature on
747 smectite dissolution rate under acidic conditions. *Geochim. Cosmochim. Acta* 69:
748 2535–2546.

749 Banerjee, A., and Merino, E., 2011. Terra rossa genesis by replacement of limestone
750 by kaolinite. III. Dynamic quantitative model. *The Journal of Geology* 119(3): 259–
751 274.

752 Barrón, V., and Torrent, J. (2002). Evidence for a simple pathway to maghemite in
753 Earth and Mars soils. *Geochimica et Cosmochimica Acta*, 66(15): 2801-2806.

754 Blanck, E., 1915. Kritische Beiträge zur Entstehung der Mediterran-Roterde. Die
755 Landwirtschaftlichen Versuchsstationen LXXXVII, Berlin: 251–314.

756 Blanck, E., 1926. Vorläufiger Bericht über die Ergebnisse einer bodenkundlichen
757 Studienreise im Gebiet der südlichen Etschbucht und des Gardasees. *Chem. Erde* 2:
758 175–208.

759 Blanck, E., Giesecke, F., Rieser, A., and Scheffer, F., 1928. Über die Entstehung der
760 Roterde im nördlichsten Verbreitungsgebiet ihres Vorkommens. *Chem. Erde* 3: 44–
761 90.

762 Blanck, E., 1930. Die Mediterran-Roterde (Terra rossa). *Handbuch der Bodenlehre* 3:
763 194-257.



764 Blanck, E., and Oldershausen, E. v., 1936. Über rezente und fossile Roterde- (Terra
765 rossa-) Bildung, insbesondere im Gebiet der südlichen Frankenalb, des
766 Altmühltales. *Chem. Erde* 10: 1–66.

767 Boero, V., and Schwertmann, U., 1987. Occurrence and transformations of iron and
768 manganese in a colluvial Terra Rossa toposequence of Northern Italy. *Catena* 14:
769 519–531.

770 Bronger, A., Ensling, J., and Kalk, E., 1984. Mineralverwitterung,
771 Tonmineralneubildung und Rubefizierung in Terra Calcis der Slowakei. *Catena* 11:
772 115–132.

773 Cornell, R., and Schwertmann, U., 2003. *The iron oxides*. Weinheim, Wiley, 616 p.

774 Danin, A., Gerson, R., Marton, K., and Garty, J., 1982. Patterns of limestone and
775 dolomite weathering by lichens and blue-green algae and their paleoclimatic
776 significance. *Palaeogeogr. Palaeoecol.* 37: 221–233.

777 DIN 19683, 1997. Deutsches Institut für Normung, Blatt 1-3, Physikalische
778 Laboruntersuchungen, Bestimmung der Korngrößenzusammensetzung nach
779 Vorbehandlung mit Natriumpyrophosphat. Berlin, Beuth Verlag. 2 p.

780 Durn, G., Ottner, F., and Slovenec, D., 1999. Mineralogical and geochemical
781 indicators of the polygenetic nature of Terra Rossa in Istria, Croatia. *Geoderma* 91:
782 125–150.

783 Fedoroff, N., Courty, M.-A., 2013. Revisiting the genesis of red Mediterranean soils.
784 *Turkish J Earth Sci.* 22: doi:10.3906/yer-1205-10.



785 Feng J.-L., Zhu, L.-P., and Cui, Z.-J., 2009. Quartz features constrain the origin of
786 terra rossa over dolomite on the Yunnan-Guizhou Plateau, China. *J. A. E. Sci.* 36(2-
787 3): 156–167.

788 Fenelon, P., 1976. Alteration en profondeur des calcaires. *Geografski Glasnik* 38: 75–
789 82.

790 Frolking, T. A., Jackson, M. L., and Knox, J. C., 1983. Origin of red clay over dolomite
791 in the loess-covered Wiscons in driftless uplands. *Soil Sci. Soc. Am. J.* 47: 817–820.

792 Günster, N., 1999. Paläopedologische Untersuchungen an pliozänen und
793 pleistozänen Sedimenten im Becken von Granada/Südspanien. *Bonner Bodenk. Abh.*
794 26, 283 p.

795 Häusler, W., and Niederbudde, E.-A., 1992. Morphologie und Alter von Böden der
796 Südlichen Frankenalb und der nichtkarbonatische Mineralbestand der Kalksteine. *Z.*
797 *Pflanzenernähr. Bodenk.* 155: 391–399.

798 Hurst, V. J., 1977. Visual estimation of iron in saprolite. *Geol. Soc. Am. Bull.* 88: 174–
799 176.

800 Ji, H., Wang, S., Ouyang, Z., Zhang, S., Sun, C., Liu, X., and Zhou, D., 2004a.
801 Geochemistry of red residua underlying dolomites in karst terrains of Yunnan-
802 Guizhou Plateau. I. The formation of the Pingba profile. *Chem. Geol.* 203: 1–27.

803 Ji, H., Wang, S., Ouyang, Z., Zhang, S., Sun, C., Liu, X., and Zhou, D., 2004b.
804 Geochemistry of red residua underlying dolomites in karst terrains of Yunnan-
805 Guizhou Plateau. II. The mobility of rare elements during weathering. *Chem. Geol.*
806 203: 29–50.



807 Klinge, H., 1958. Eine Stellungnahme zur Altersfrage von Terra-rossa-Vorkommen
808 (Unter besonderer Berücksichtigung der Iberischen Halbinsel, der Balearischen
809 Inseln und Marokkos). *Z. Pflanzenernähr. Düng. Bodenk.* 81(1): 56–63.

810 Küfmann, C., 2008. Are Cambisols in Alpine Karst Autochthonous or Eolian in Origin?
811 *Arctic Ant. Alp. Res.* 40(3): 506-518.

812 Kubiëna, W., 1945. Beiträge zur Bodenentwicklungslehre: Der Kalksteinbraunlehm
813 (Terra Fusca) als Glied der Entwicklungsserie der mitteleuropäischen Rendsina. *Z.*
814 *Pflanzenernähr. Düng. Bodenk.* 35(1-4): 22–45.

815 Laverty, M., 2012. Preparing the ground - new mechanisms for karst and
816 speleogenesis: 'altération', fantomisation and replacement. *Cave Karst Sc.* 39(2): 72–
817 76.

818 Leiningen, W., Graf zu, 1915. Über die Einflüsse von äolischer Zufuhr für die
819 Bodenbildung. *Mitt. Geol. Ges. Wien* 7: 139–177.

820 Leiningen, W., Graf zu, 1930. Die Roterde (Terra Rossa) als Lösungsrest mariner
821 Kalkgesteine. *Chem. Erde* 4: 178–187.

822 Lucke, B., 2008. Demise of the Decapolis. Past and present desertification in the
823 context of soil development, land use and climate. Saarbrücken, AkademikerVerlag,
824 231p.

825 Lucke, B., Kemnitz, H., and Bäumler, R., 2012. Evidence for isovolumetric
826 replacement in some Terra Rossa profiles of northern Jordan. *Bull. Mex. Geol. Soc.*
827 64: 31–45.



828 Lucke, B., Kemnitz, H., Bäumler, R., and Schmidt, M., 2014. Red Mediterranean soils
829 in Jordan: new insights in their origin, genesis, and role as environmental archives.
830 *Catena* 112: 4–24.

831 Lucke, B., and Sprafke, T., 2015. Correlation of soil color, redness ratings, and
832 weathering indices of *Terra Calcis* along a precipitation gradient in northern Jordan.
833 In: Lucke, B., Bäumler, R., Schmidt, M. (eds.), *Soils and Sediments as Archives of*
834 *Environmental Change. Geoarchaeology and Landscape Change in the Subtropics*
835 and *Tropics*. Fränkische Geographische Gesellschaft, Erlangen: 53-68.

836 Lucke, B., Schmidt, U., 2015. Grain size analysis of calcareous soils and sediments:
837 inter-method comparison with and without calcium carbonate removal. In Lucke, B.,
838 Bäumler, R., and Schmidt, M. (eds.), *Soils and Sediments as Archives of*
839 *Environmental change. Geoarchaeology and Landscape Change in the Subtropics*
840 and *Tropics*. Erlangen, Franconian Geographical Society: 83-96.

841 Maliva, R., and Siever, R., 1988. Diagenetic replacement controlled by force of
842 crystallization. *Geology* 16: 688–691.

843 Martin, J.-M., Elbaz-Poulichet, F., Guieu, C., Loyer-Pilot, M.-D., and Han, G., 1989.
844 River versus atmospheric input of material to the mediterranean sea: An overview.
845 *Mar. Chem.* 28(1-3): 159–182.

846 Merino, E., Banerjee, A., 2008. Terra Rossa genesis, implications for Karst, and
847 eolian dust: A geodynamic thread. *J. Geol.* 116: 62–75.

848 Meert, J., Pruett, F., and Merino, E., 2009. An “Inverse Conglomerate” Paleomagnetic
849 Test and Timing of *In Situ* Terra Rossa Formation at Bloomington, Indiana. *J. Geol.*
850 117: 126-138.



851 Meyer, B., 1979. Die Entcarbonatisierungsrötung als bodengenetischer Teilprozeß.
852 Mittlg. dt. bodenkundl. Ges. 29-II: 705-708.

853 Monroe, W. H., 1986. Examples of the replacement of limestone by clay. *Miss. Geol.*
854 7: 1–6.

855 Moresi, M., and Mongelli, G., 1988. The relation between the Terra Rossa and the
856 carbonate-free residue of the underlying limestones and dolostones in Apulia, Italy.
857 *Clay Miner.* 23: 439–446.

858 Mortland, M. M., and Raman, K. V., 1968. Surface acidity of smectites in relation to
859 hydration, exchangeable cation, and structure. *Clays and Clay Minerals* 16(5): 393-
860 398.

861 Mückenhausen, E., Beckmann, H., Schröder, D., and Stephan, S., 1975. Relikte von
862 Paläoböden, Spalten- und Dolinen-Füllungen in carbonatischen Gesteinen der
863 nördlichen Eifel. *Catena* 2: 95–106.

864 Muhs, D., 2001. Evolution of soils on Quaternary reef terraces of Barbados, West
865 Indies. *Quat. Res.* 56: 66–78.

866 Muhs, D. R., Budahn, J., Prospero, J. M., and Carey, S. N., 2007. Geochemical
867 evidence for African dust inputs to soils of western Atlantic islands: Barbados, the
868 Bahamas and Florida. *J. Geophys. Res.* 112: 1–26.

869 Ostrom, M. E., 1961. Separation of clay minerals from carbonate rocks by using acid.
870 *J. Sed. Pet.* 31(1): 123–129.



871 Prognon, F., Cojan, I., Kindler, P., Thirdy, M., and Demange, M., 2011. Mineralogical
872 evidence for a local volcanic origin of the parent material of Bermuda Quaternary
873 paleosols. *Quat. Res.* 75: 256–266.

874 Rabenhorst, M. C., and Wilding, L. P., 1984. Rapid method to obtain carbonate-free
875 residues from limestone and petrocalcic materials. *Soil Sci. Soc. Am. J.* 48: 216–219.

876 Reifenberg, A., 1927. Über die Rolle der Kieselsäure als Schutzkolloid bei der
877 Entstehung mediterraner Roterden. *Z. Pflanzenernähr. Düng. Bodenk.* 10: 159–186.

878 Reifenberg, A., 1947. The soils of Palestine. London, T. Murby, 179 p.

879 Ross, C.S., and Stephenson, L.W., 1939. Calcareous shells replaced by beidellite.
880 *Am. Mineral.* 24: 393–397.

881 Schlichting, E., Blume, H.-P., and Stahr, K., 1995. *Bodenkundliches Praktikum*. 2nd
882 ed. Berlin, Blackwell Wissenschafts-Verlag, 295 p.

883 Schmidt, M., Lucke, B., Bäumler, R., al-Saad, Z., al-Qudah, B., Hutcheon, A., 2006.
884 The Decapolis region (Northern Jordan) as historical example of desertification?
885 Evidence from soil development and distribution. *Quat. Intl.* 151: 74-86.

886 Schwertmann, U., Murad, G., Schulze, D.G., 1982. Is there holocene reddening
887 (haematite formation) in soils of axeric temperature areas? *Geoderma* 27: 209-223.

888 Shijie, W., Hongbing, J., Ziyuan, O., Deqan, Z., Leping, Z., and Tingyu, L., 1999.
889 Preliminary study on weathering and pedogenesis of carbonate rock. *Sci. China Ser.*
890 D. 42(6): 572–581.

891 Skowronek, A., 2016. *Terra calcis. Handbuch der Bodenkunde*, Kap. 3.3.2.9, 1-38.



892 Stephenson, L. W., 1939. Fossil mollusks preserved as clay replacements near
893 Pontotoc, Mississippi. *J. Paleontol.* 13: 96–99.

894 Temur, S., Orhan, H., and Deli, A., 2009. Geochemistry of the limestone of Mortas
895 Formation and related Terra Rossa, Seydisehir, Konya, Turkey. *Geochem. Intl.* 47:
896 67–93.

897 Terefe, T., Mariscal-Sancho, I., Peregrina, F., and Espejo, R., 2008. Influence of
898 heating on various properties of six Mediterranean soils. A laboratory study.
899 *Geoderma* 143(3): 273-280.

900 Torrent, J., Barrón, V., and Liu, Q., 2006. Magnetic enhancement is linked to and
901 precedes hematite formation in aerobic soil. *Geophysical Research Letters*, 33(2):
902 DOI: 10.1029/2005GL024818.

903 Trappe, M., 2011. *Sedimentpetrographie, Gliederung und Genese von
904 Karstsedimenten, dargestellt am Beispiel der Südlichen Frankenalb.* Stuttgart,
905 Schweizerbart Borntraeger Science Publishers, 195 pp.

906 TUM, 2014. *Technische Universität München, Geomorphologie und Bodenkunde:
907 Bodenlehrpfad Schwaighauser Forst.* <http://www.geo.wzw.tum.de/> [31-08-2015].

908 Verboom, W., Pate, J., and Aspandiar, M., 2009. Neoformation of clay in lateral root
909 catchments of mallee eucalypts: a chemical perspective. *Ann. Bot.* 105(1): 23–36.

910 Weyl, P. K., 1959. Pressure solution and the force of crystallization: a
911 phenomenological theory. *Journal of Geophysical Research* 64: 2001–2025.



912 WRB 2014. World Reference Base for Soil Resources 2014. International soil
913 classification system for naming soils and creating legends for soil maps. W. S. Res.
914 Rep. 106. Rome, FAO, 181 p.

915 Yaalon, D., and Ganor, E., 1973. The influence of dust on soils during the
916 Quaternary. *Soil Sci.* 116: 146–155.

917 Zhu, L., and Li, J., 2002. Metasomatic mechanism of weathering-pedogenesis of
918 carbonate rocks: I. Mineralogical and micro-textural evidence. *Chin. J. Geochem.*
919 21(4): 334–339.

920 Zech, W., Wilke, B.-M., and Drexler, O., 1979. Analytische Kennzeichnung von
921 Karstschlotten-Füllungen in der Fränkischen Alb. *Z. Geomorph. N.F.*, Suppl.-Bd. 33:
922 182-193.

923 Zippe, W., 1854. Einige geognostische und mineralogische Bemerkungen über den
924 Höhlenkalkstein des Karst. In Schmidl, A.: *Die Grotten und Höhlen von Adelsberg*,
925 Lueg, Planina und Laas. Pleiades Publishing Ltd., Vienna: 209-221.

926

927

928 **Figure and table captions**

929



930



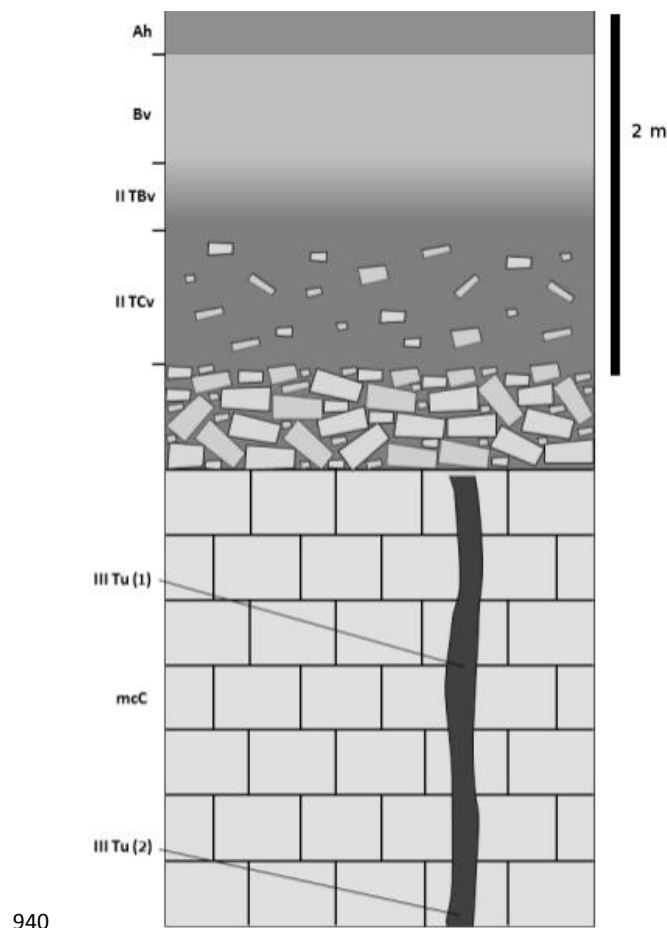
931 Figure 1: Map showing the location of the investigated profiles in Franconia, and the
932 region inside Germany. Map based on www.openstreetmaps.org (Open Database
933 License, ©OpenStreetMap contributors).



934 Figure 2a: The profile "Fricke" sampled near Weißenburg i. Bayern. The left side
935 shows the upper part of the profile, which connects to the lower part shown on the
936 right side as indicated by the rectangle. Due to a step-wise exposition of rock cuts in



937 the quarry, it was not possible to obtain a picture showing the whole profile. Sampling
938 locations are marked by the horizon labels. Each mark on the meter tape represents
939 10 cm.



941 Figure 2b: Schematic drawing of the profile "Fricke" for a better illustration of soil
942 horizons.

943

944

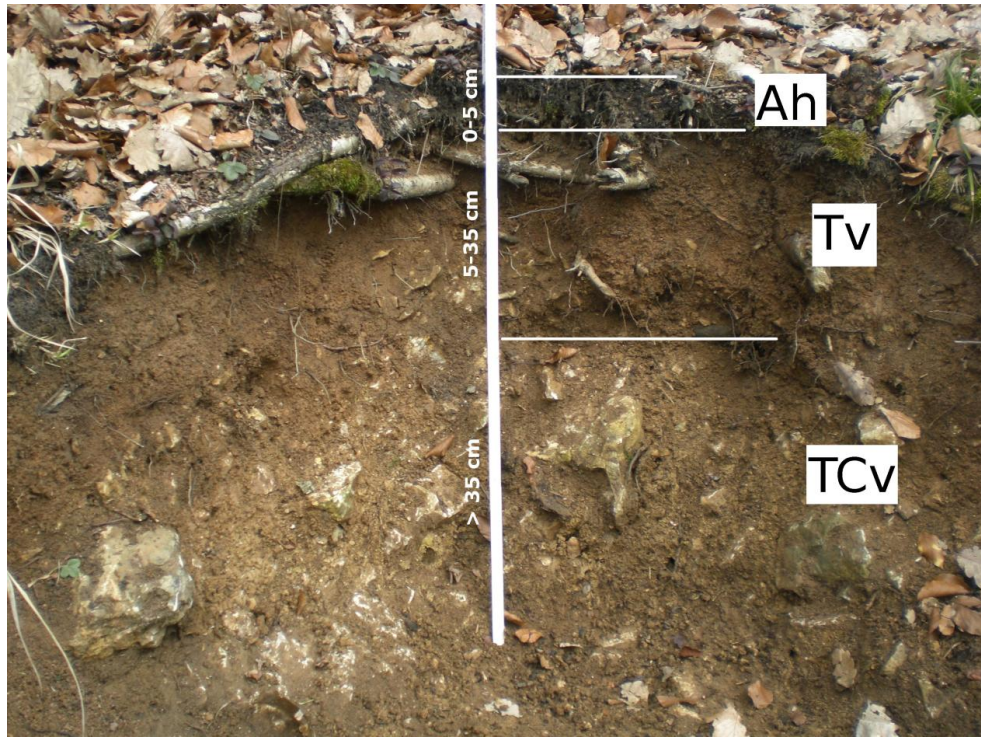


945

946

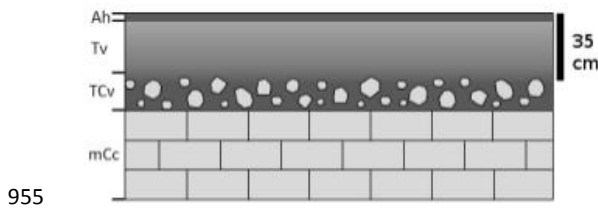
947 Figure 2c: Close-up of crack infillings. The red clay is homogeneous throughout,
948 there are no horizons, and no indicators of fluvial deposition could be observed.
949 Transition to bedrock occurs in a zone of 'powdery' limestone of about 1 mm
950 thickness as described earlier for other crack fills by Trappe (2011).

951



952

953 Figure 3a: The profile "Schwaighauser Forst" near Regensburg. Sampling locations
954 are indicated by the horizon labels, and soil depths are marked along the white bar.

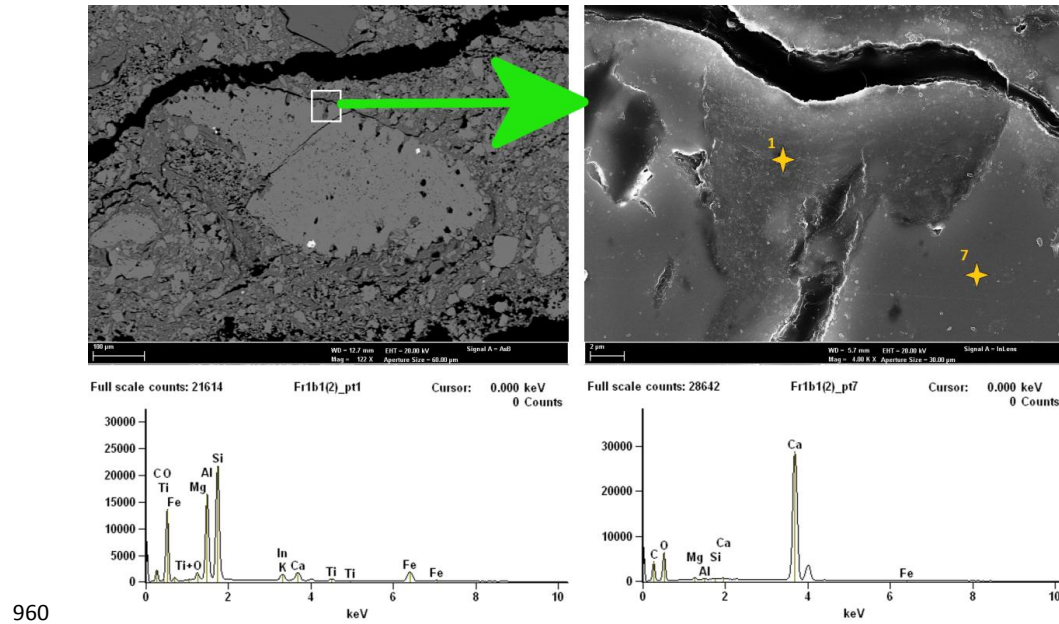


955

956 Figure 3b: Schematic drawing of the profile "Fricke" for a better illustration of soil
957 horizons.

958

959



961 Figure 4: Calcite grain starting to be replaced by clay in the rock-soil transition zone
962 of the Terra Rossa limestone crack fillings in the profile "Fricke". Right is an
963 enlargement of the square marked on the left. The geochemical composition
964 determined by EDS is shown at the bottom for point 1 (left) and point 7 (right),
965 indicating that clay formation maintaining the original bedding structure took place in
966 the darker area of the calcite grain.

967

968

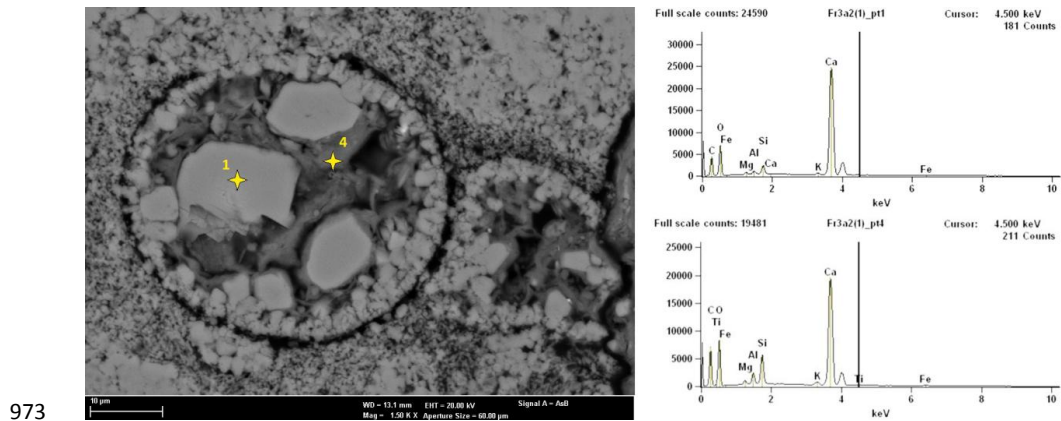
969

970

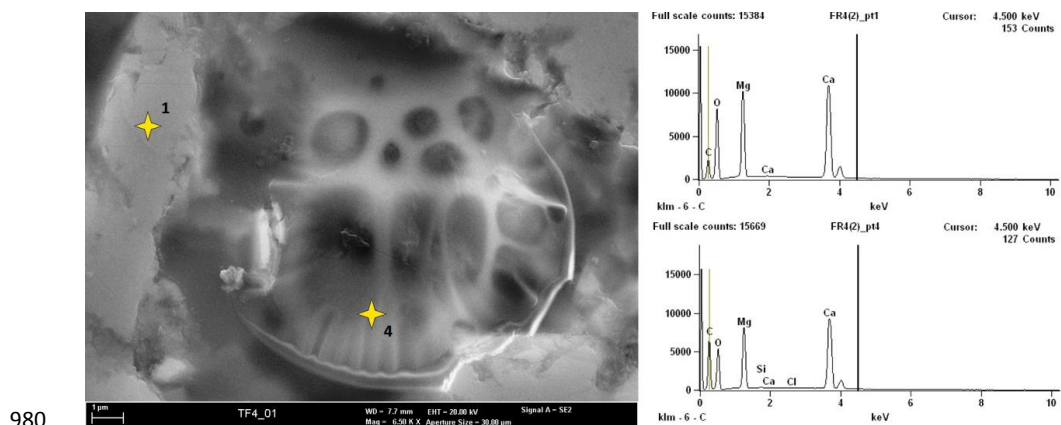
971



972



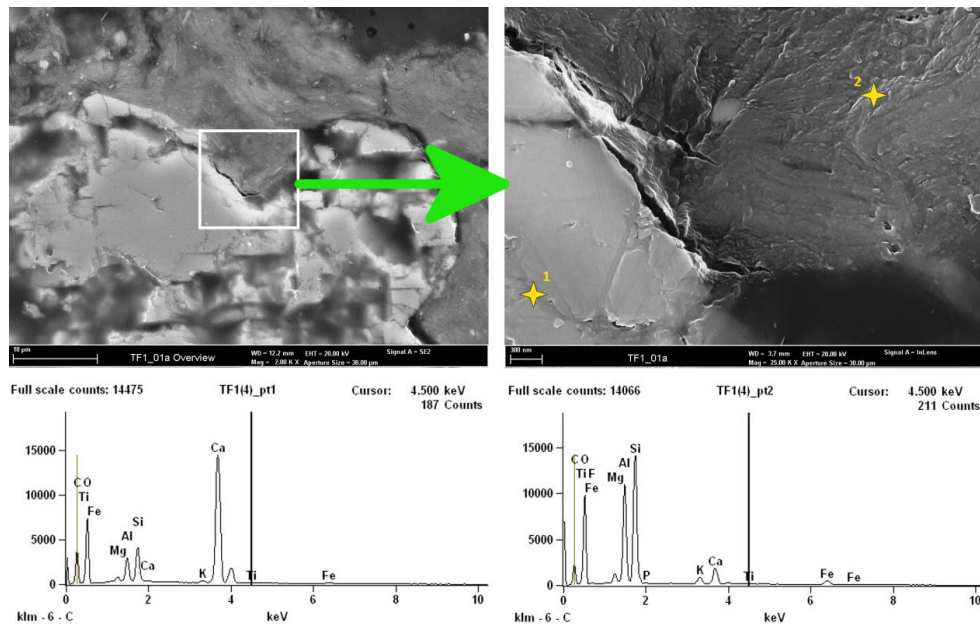
974 Figure 5: Round microfossil partially filled with amorphous clay in the rock-soil
 975 transition zone of the Terra Rossa limestone crack fillings in the profile "Fricke". The
 976 geochemical composition determined by EDS is shown to the right for point 1 (above)
 977 and point 4 (below), indicating that part of the inner microfossil consists of clay
 978 although there are no traces of crystalline allochthonous clay or cracks in the fossil's
 979 shell.





981 Figure 6: Remains of a microfossil in the rock-soil transition zone of the dolomitic
982 limestone of the "Schwaighauser Forst" profile. EDS-analyses demonstrate the high
983 magnesium context of the rock (point 1, top right), but also show a slight increase of
984 Si and decrease of Ca and Mg in the darker areas inside the microfossil, indicating a
985 beginning of clay formation (point 4, bottom right).

986

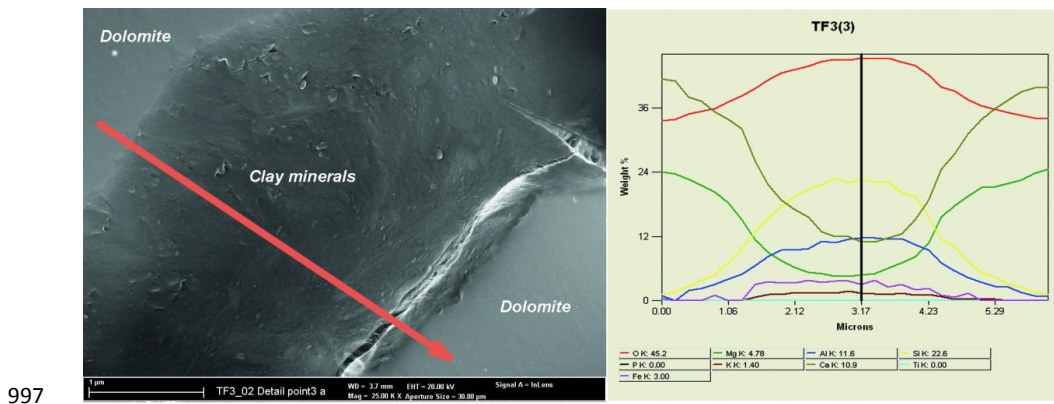


988 Figure 7: Calcite grain starting to be replaced by clay in the rock-soil transition zone
989 of the Terra Fusca in the profile "Schwaighauser Forst". Right is an enlargement of
990 the square marked on the left. The geochemical composition determined by EDS is
991 shown at the bottom for point 1 (left) and point 2 (right), indicating that clay formation
992 started inside small cracks of the calcite grain, although chemically still dominated by
993 Ca (point 1). In contrast, the soil matrix in the larger fissure is characterized by a
994 further increase of Si, Al, and Fe, while Ca was diminished (point 2).

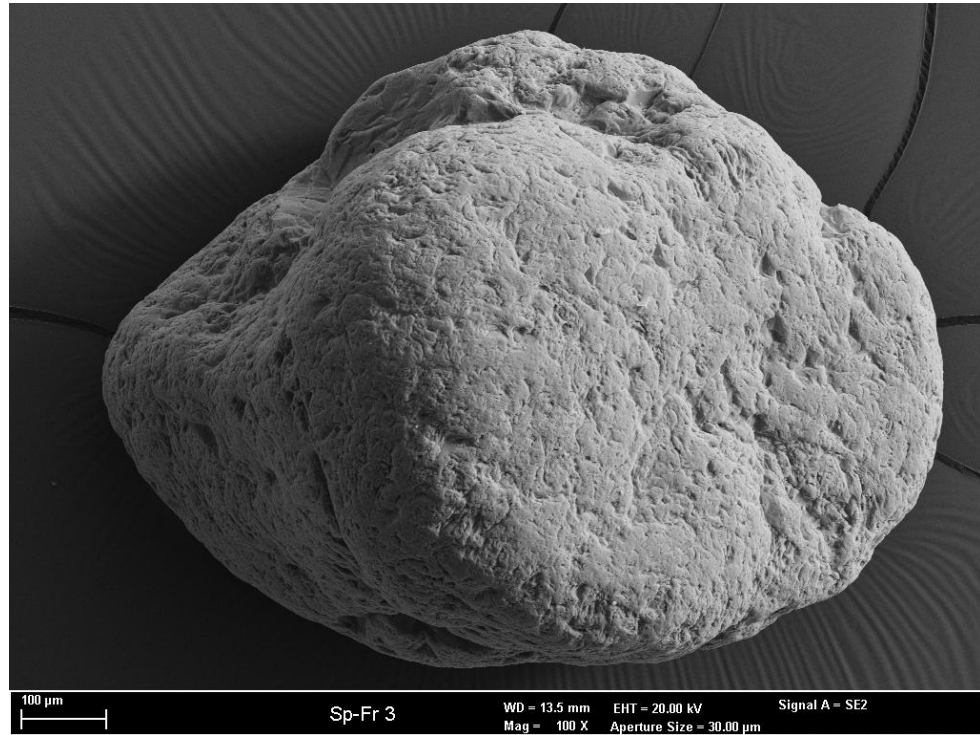


995

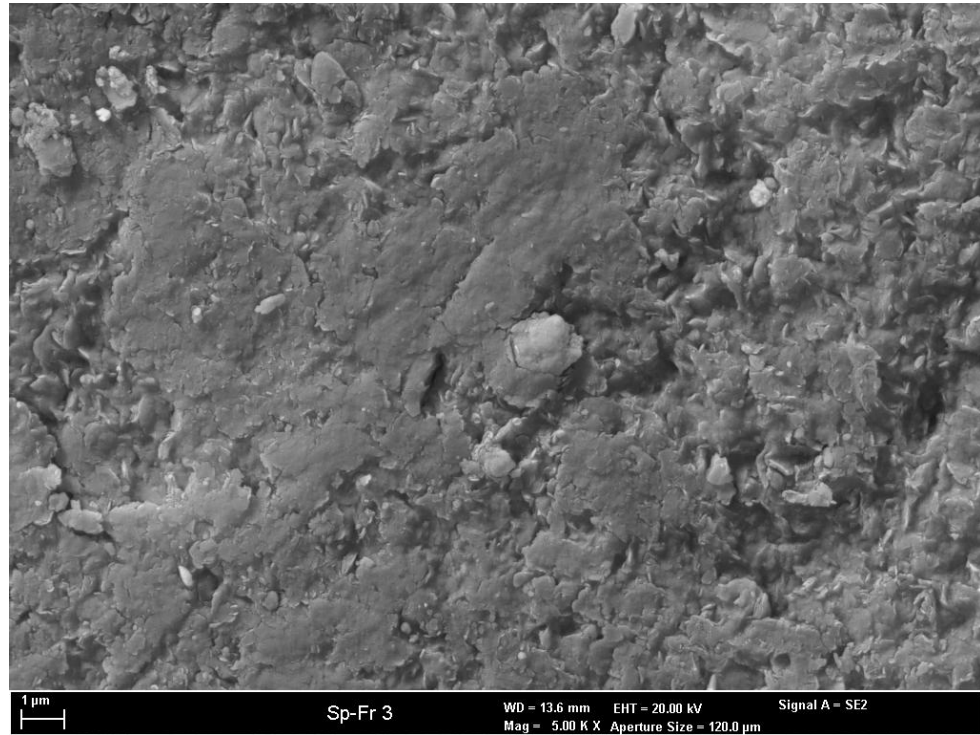
996



997
998 Figure 8: SEM cross-section using EDS to determine element composition along a
999 section of a dolomite grain in the rock-soil transition zone of the Terra fusca in the
1000 profile "Schwaighauser Forst". The graph to the right shows the weight % of the
1001 studied elements along the section marked by the arrow to the left. As can be seen,
1002 there is a gradual increase of Si, Al, and Fe towards the darker area of the dolomite
1003 grain, while Ca and Mg are reduced, pointing to gradual isovolumetric replacement of
1004 the dolomite by clay minerals.



1006 Figure 9: Quartz grain of the coarse sand fraction of the red fill in the limestone crack
1007 of the Fricke profile. Note the densely set small V-shaped marks typical for aeolian
1008 transport during loess deposition.



1009

1010 Figure 10: Grain from the fine sand fraction of the red fill in the limestone crack of the
1011 Fricke profile. It is completely covered by clay, possibly representing a pseudosand
1012 aggregate largely consisting of clay (and silt).

1013

1014

1015 Table 1: Results of bulk soil analyses of the profiles "Fricke" and "Schwaighauser
1016 Forst". The Fe (d/t) ratio describes the ratio of dithionite-soluble iron (Fe_d) to total iron
1017 contents. Increasing redness is reflected by smaller values in the index according to
1018 Hurst (1977). The dolomite content of the bedrock at the Schwaighauser Forst profile
1019 was calculated according to the residue mass after the rock's dissolution with HCl.



Sampling depth [cm]	Sample	Munsell dry	RR after Hurst (dry)	Oxalat-soluble silicium [mg/g]	Dithionite-soluble iron [mg/g]	C _{org} %	pH	CaCO ₃ %	Clay %	Silt %	Sand %	Fe(d/t)	Ti/Zr
Profile FRICKE													
0-25	Ah	10 YR 6/3	40	0.01	11.5	3.08	4.5	2.1	27	69	4	0.49	9
25-90	Bv	10 YR 6/4	30	0.14	17.5	0.28	4.7	1.5	36	61	3	0.47	11
90-125	II TBv	10 YR 6/4	30	0.03	19.1	0.32	5.5	0.5	45	52	3	0.43	12
125-200	II Tcv	10 YR 6/4	30	0.07	26.6	0.35	6.7	0.6	59	38	3	0.54	15
370	III Tu (1)	5 YR 4/4	15	0.77	33.6	0.13	7.7	2.1	65	22	13	0.5	18
520	III Tu (2)	5 YR 4/4	15	0.75	33.0	0.12	7.6	1.6	66	21	13	0.49	15
500	mC	10 YR 5/3	33	-	-	-	98.1	75	24	1	-	-	20
Profile SCHWAIGHAUSER FORST													
0-5	Ah	10 YR 6/3	40	0.02	10.1	3.80	6.5	4.6	39	39	22	0.38	11
5-35	Tv	10 YR 6/4	30	0.04	14.3	1.10	7.6	3.2	57	28	15	0.43	13
>35	Tcv	10 YR 7/4	35	0.06	9.9	1.40	7.6	35.2	67	23	10	0.49	21
>50	mC	10 YR 4/2	40	-	-	-	(99.99)	86	13	1	-	-	11

Table 1: Results of bulk soil analyses of the profiles "Fricke" and "Schwaighauser Forst". The Fe(d/t) ratio describes the ratio of dithionite-soluble iron (Fe_d) to total iron contents. Increasing redness is reflected by smaller values in the index according to Hurst (1977). The dolomite content of the bedrock at the Schwaighauser Forst profile was calculated according to the residue mass after the rock's dissolution with HCl.